Journal of Magnetic Resonance 307 (2019) 106576

Contents lists available at ScienceDirect

Journal of Magnetic Resonance

journal homepage: www.elsevier.com/locate/jmr

Non-uniform HYSCORE: Measurement, processing and analysis with Hyscorean

Luis Fábregas Ibáñez [a], Janne Soetbeer [a], Daniel Klose [a], Matthias Tinzl [b], Donald Hilvert [b], Gunnar Jeschke [a,*]

[a] ETH Zurich, Laboratory of Physical Chemistry, Vladimir-Prelog-Weg 2, 8093 Zurich, Switzerland
[b] ETH Zurich Laboratory of Organic Chemistry, Vladimir-Prelog-Weg 3, 8093 Zurich, Switzerland

ARTICLE INFO

Article history:
Received 29 May 2019
Revised 13 August 2019
Accepted 15 August 2019
Available online 19 August 2019

Keywords:
Non-uniform sampling
NUS
EPR
HYSCORE
NUS HYSCORE
maxEnt
IST
CAMERA

ABSTRACT

Non-uniform sampling (NUS) provides a considerable reduction of measurement time especially for multi-dimensional experiments. This comes at the cost of additional signal processing steps to reconstruct the complete signal from the experimental data points. Despite being routinely employed in NMR for many experiments, EPR applications have not benefited from NUS due to the lack of a straightforward implementation to perform NUS in common commercial spectrometers. In this work we present a novel method to perform NUS HYSCORE experiments on commercial Bruker EPR spectrometers, along with a benchmark of modern reconstruction methods, and new processing software tools for NUS HYSCORE signals. All of this comes in the form of a free-software package: Hyscorean. Experimental NUS spectra are measured and processed with this package using different reconstruction methods and compared to their uniform sampled counterparts, thereby showcasing the method's potential for EPR spectroscopy.

1. Introduction

In EPR spectroscopy, multi-dimensional experiments, foremost the two-dimensional hyperfine sublevel correlation (HYSCORE) experiment, play a pivotal role in the study of hyperfine couplings in a variety of electron-nuclear spin systems [1]. Generally, in conventional uniformly sampled methods, the potential resolution and sensitivity are limited by the time required to complete the experiments. With limited measurement time at hand, spectroscopists tend to find a balance between digital resolution and signal-to-noise ratio to match the given time constraints. Non-uniform sampling (NUS) opens the possibility to sample a subset of the original data as a means to potentially improve spectral resolution and sensitivity at given measurement time or to reduce measurement time at given sensitivity and resolution.

This reduction comes at the price of additional processing steps before reaching a final spectrum. The standard processing technique for the approximate analysis of frequencies for a uniformly-sampled signal is the Fourier transform. Instead, for NUS signals, this transform no longer corresponds to an expansion into an orthonormal Fourier basis set [2]. The consequences can be considered as follows. When the sampling times are specified with finite precision (as is the case on all commercial spectrometers) a uniform grid can be defined on which all samples will fall [3,4]. The positions in the grid at which the timings fall form the so-called NUS grid or schedule. The relationship between the NUS signal and the spectrum is particularly simple when the sampling is restricted to such a regular grid [5] (see Fig. 1). Direct Fourier transform (DFT) of the zero-augmented signal (i.e. a NUS signal where all non-measured points are set to zero) will result in convolution of the true spectrum with the point-spread function (PSF) of the sampling schedule [4,6]. We will refer to spectra obtained this way as non-uniform DFT (nuDFT) spectra. This convolution results in strong aliasing artifacts known as sampling artifacts [4] or intra-band aliases [2]. To remove the sampling artifacts and obtain the true spectrum, non-Fourier methods of spectral analysis must be employed. Such methods aim to reconstruct the missing points in the signal via some optimization of a regularization functional, subject to a data consistency constraint. These so-called reconstruction methods include multidimensional decomposition [7,8], iterative soft thresholding [9–13], maximum entropy [14,4] and non-uniform fast-Fourier transform [15–17].

In an effort to minimize the introduction of the aforementioned artifacts, the PSFs of different NUS grids have been extensively

* Corresponding author.
E-mail address: gjeschke@ethz.ch (G. Jeschke).

https://doi.org/10.1016/j.jmr.2019.106576
1090-7807/

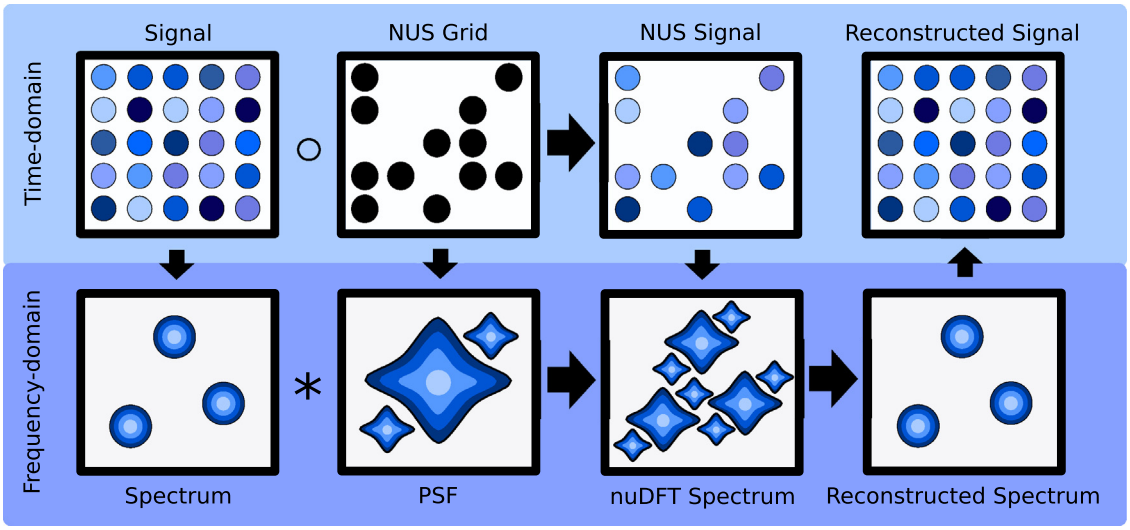

Fig. 1. Role of the NUS sampling grid and the PSF. In time-domain, the NUS signal is equivalent to the Hadamard multiplication of the signal with the NUS grid. In frequency-domain, this same process is equivalent to convolution of the true spectrum with the PSF of the NUS grid. In both cases a spectrum is obtained, which contains the true spectrum and sampling artifacts which can be removed by reconstruction methods.

studied [18–20]. The inclusion of randomness was identified as one of the most relevant factors in NUS grid design, as the resulting sampling artifacts appear noise-like in the spectra [4,5,21]. However, the relative intensities of the sampling artifacts depend on the specifics of the NUS grid employed. Further work to improve the sensitivity of NUS spectra has been carried out in the form of envelope-matched sampling (EMS) [4,20,22] and beat-matched sampling (BMS) [4,22], where the random sampling is matched to some probability density function, e.g. an exponential function matched to the signal decay [21,23]. Despite all efforts, to date there is still no complete understanding of the optimal design of NUS sampling schemes [4].

Originating from the radio astronomy field, NUS and its reconstruction methods have matured in the field of NMR and have found already many applications [24,25]. In the field of EPR spectroscopy, NUS had not found any interest until Nakka et al. [26] proposed two different sampling schemes for NUS HYSCORE measurements along with maximum entropy reconstruction in silico. The acquisition times were estimated to reduce by an order of magnitude, without experimental proof due to lacking implementation on commercial spectrometers. Recently, a first proposal on the optimization of the NUS reconstruction has been presented by Motygullina et al. [27], yet still without experimental proof.

In this work we present a novel methodology to perform NUS HYSCORE experiments on commercial Bruker spectrometers as well as a benchmark study of different modern reconstruction methods. We also present new signal processing tools, which allow a more precise and validated processing of the NUS signals to their corresponding spectra. All these new developments come integrated in a new free-software package: Hyscorean. It generates NUS schedules, provides PulseSPEL programms for NUS measurements on Bruker spectrometers and can perform full processing and analysis of uniform and non-uniform sampled HYSCORE spectra.

2. Non-Fourier methods of spectral analysis

As discussed above, due to the poor applicability of the DFT for the analysis of NUS signals, alternative spectral analysis methods must be employed. These methods reconstruct the spectrum and the missing points in the NUS signal. This is achieved by optimization of a certain regularization term under the constraint that the inverse DFT of the spectrum is consistent with the experimental NUS data. The regularization is performed by minimization of an objective function of the form

$$\mathbf{X} = \underset{\mathbf{X}}{\operatorname{argmin}} \left\{ \lambda \|\mathbf{b} - \mathbf{DFX}\|_2 - P(\mathbf{X}) \right\} \tag{1}$$

where $\mathbf{X}$ is the spectrum, $\mathbf{b}$ is the zero-augmented experimental NUS signal, $\mathbf{F}$ is the inverse Fourier transform kernel, $\mathbf{D}$ is the NUS grid, $P(\mathbf{X})$ is the regularization penalty term and λ the Lagrange multiplier. Due to the regularization nature of spectral reconstruction, the intensity response of these methods is non-linear. However, the choice of method and regularization parameter modulates the extent of this non-linearity. For this work we have considered two different families of reconstruction methods, which differ in their regularization criteria: iterative soft-thresholding and maximum entropy reconstruction methods.

2.1. Iterative soft-thresholding

The iterative soft-thresholding (IST) methods are based on the compressed-sensing principle [9]. This states that a sub-Nyquist sampled signal can be recovered by exploiting its spectral sparsity through optimization. As ℓ_1-regularization methods, these employ a spectral sparsity penalty as a regularization term in the minimization functional

$$\mathbf{X}_{\mathrm{IST}} = \underset{\mathbf{X}}{\operatorname{argmin}} \left\{ \lambda \|\mathbf{b} - \mathbf{DFX}\|_2 - \|\mathbf{X}\|_1 \right\}. \tag{2}$$

IST methods solve this functional by iteratively updating the spectrum $\mathbf{X}$ with all values of $\mathbf{F}^{-1}\mathbf{b}$ (i.e. the nuDFT spectrum) being larger than a threshold value η. Following the recommendations of [11,12] the threshold is gradually reduced at each iteration with a scaling factor of 0.98. Furthermore, the input signal is also updated at each iteration, by subtracting either the term $\mathbf{DFX}$ or $(1-\mathbf{D})\mathbf{FX}$. There are, thus, two different IST variations [12]: Drori IST (IST-D) [10] and Stern IST (IST-S) [13]. In IST-D the term $\mathbf{DFX}$ is employed so that the measured points in $\mathbf{b}$ are updated and all non-measured points are left at zero. This allows the method to find a balance between data agreement and sparsity of the solution. In IST-S the term $(1-\mathbf{D})\mathbf{FX}$ is employed so that non-measured points are updated and all measured points are left unchanged. This enforces strict

accordance between the reconstruction and the experimental data. The enforcement of data agreement present in both IST methods results in a quasi-linear intensity response of the reconstructed spectrum with respect to the experimental data, which may allow the recovery of less intensive features of the spectra. Quasi-linearity is a consequence of strict preservation of experimental data and comes at the cost of increased likelihood of introducing spectral artifacts in the reconstructed spectra [28,29]. Please note that the IST-S method (as proposed by Stern et al. [13]) allows some tunability of the non-linearity by specification of an accuracy parameter. Still, in this work we considered only the operation of the IST method in the quasi-linear regime.

2.2. Maximum entropy

Maximum entropy (maxEnt) methods aim to find an optimally reconstructed spectrum, which exhibits minimal statistical information content, i.e. maximal entropy [14]. From all reconstruction methods, maxEnt methods were the first ones applied and studied in NMR, where they have been widely used [4,28]. These methods employ an entropy penalty $S(\mathbf{X})$ as the regularization term, i.e.

$$\mathbf{X}_{\text{maxEnt}} = \underset{\mathbf{x}}{\operatorname{argmin}} \{\lambda \|\mathbf{b} - \mathbf{DFX}\|_2 - S(\mathbf{X})\}. \tag{3}$$

The entropy of choice is the Hoch-Hore entropy, which in contrast to the older Shannon and Skilling entropies, is strictly convex (ensuring unique results) and insensitive to the phase of the signal [28,30,31]. The latter property is especially valuable for HYSCORE data, where analysis of the frequency and magnitude spectra determine the phase in a non-trivial way. The Hoch-Hore entropy penalty is given by

$$S(\mathbf{X}) = -\sum_{i=1}^{N} |X_i| \log\left[\frac{|X_i|}{\delta} + \sqrt{1 + \left(\frac{|X_i|}{\delta}\right)^2}\right] - \sqrt{|X_i|^2 + 4\delta^2} \tag{4}$$

where δ is the so-called background parameter, which to a large extent determines the threshold of λ at which the intensity response of the reconstruction becomes significantly non-linear. It also controls the curvature of the maxEnt functionals [28], with smaller δ-values leading to smoother functionals. The value of the Lagrange multiplier λ in (3) controls the linearity of the intensity response. Large values of λ lead to quasi-linear reconstruction, whereas smaller values lead to non-linear reconstruction. While quasi-linearity comes at the cost of increased likelihood of introducing spectral artifacts, non-linearity allows for the recovery of significant signals from highly noisy NUS spectra, yet at the risk of suppressing significant peaks with weak intensities.

The fast-forward maxEnt (FFM) [32] reconstruction method represents the limit $\lambda \to \infty$, where experimental data are employed as measured and only the missing points are optimized,

$$\mathbf{X}_{\text{FFM}} = \operatorname{argmin}_{\mathbf{X}}\{S(\mathbf{X})\}. \tag{5}$$

hence enforcing a strict data accordance and resulting in quasi-linearity of the intensity response. Furthermore, this simplifies the parameter space to just the background parameter for the entropy functional. However, this method is known to overfit experimental data especially at low signal-to-noise ratio (SNR) [4]. Reconstruction is achieved by minimization of the entropy gradient of the spectrum, either by conjugate gradient (FFM-CG) or gradient descent (FFM-GD) minimization.

2.2.1. CAMERA

The convex accelerated maximum entropy reconstruction method (CAMERA) is a fast, flexible and highly tunable maxEnt reconstruction method [28]. CAMERA is an implementation of Nesterov's accelerated first-order optimization algorithm [33,34] applied to the maxEnt problem (3) and can be operated in two modes. In the constant-aim mode CAMERA updates its Lagrange multiplier λ at each iteration until it reaches a certain optimal value λ^* [28]. In its constant-λ mode, the Lagrange multiplier is kept constant at a given value. When this value λ is chosen near λ^*, the results remain unchanged. However, the potential in this mode resides in the possibility to choose $\lambda \ll \lambda^*$, which results in highly non-linear reconstructions.

3. Post-processing of NUS HYSCORE data

Besides the reconstruction of the NUS signals and their spectra, further improvement can be obtained by additional signal processing steps. Reconstruction is not perfect and sometimes strong sampling artifacts may still be present in the reconstructed spectrum. Furthermore, highly non-linear reconstruction may remove some true signals from the spectrum. This introduces an uncertainty in the NUS spectra which, if untreated, may leave the method non-applicable to complex systems of interest. We present here two signal processing tools, which aim to reduce the uncertainty in NUS spectra.

3.1. Spectral symmetrization

Due to the nature of the HYSCORE experiment, all spectra are expected to exhibit symmetry about their diagonal or anti-diagonal. In practice, some asymmetry is occasionally observed even in high-quality data, but this effect is not very well understood and disregarded in further analysis. Each crosspeak in the spectrum should be accompanied by a mirror image with respect to the diagonal (weak-coupling regime) or anti-diagonal (strong-coupling regime). The sampling artifacts introduced by the NUS in the spectrum are, however, random in nature and asymmetric. Therefore, by imposing symmetry upon the spectrum, any sampling artifacts remaining in the spectrum are strongly suppressed, while retaining all true crosspeaks (see Fig. 2). The symmetrization of the HYSCORE spectrum is achieved through geometric averaging,

$$\mathbf{X}_{\text{Symmetric}} = \Lambda\left(\Lambda\mathbf{X}(\Lambda\mathbf{X})^T\right)^{1/2}, \tag{6}$$

where Λ is a matrix manipulation operator. In comparison to the arithmetic averaging proposed in [27], stronger artifact suppression is obtained by geometric averaging. For the symmetrization about

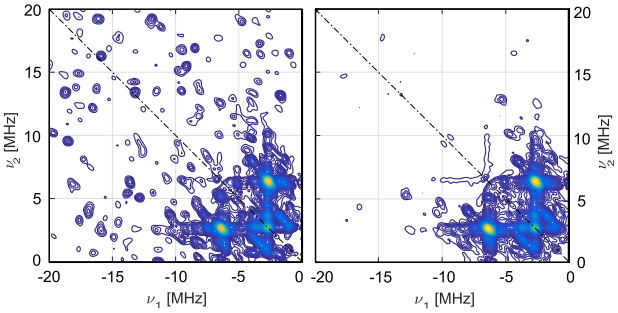

Fig. 2. Example of the effects of spectral symmetrization (along both the diagonal and anti-diagonal) on a region of a HYSCORE spectrum with strong sampling artifacts (left) before and (right) after, where the artifacts are strongly reduced.

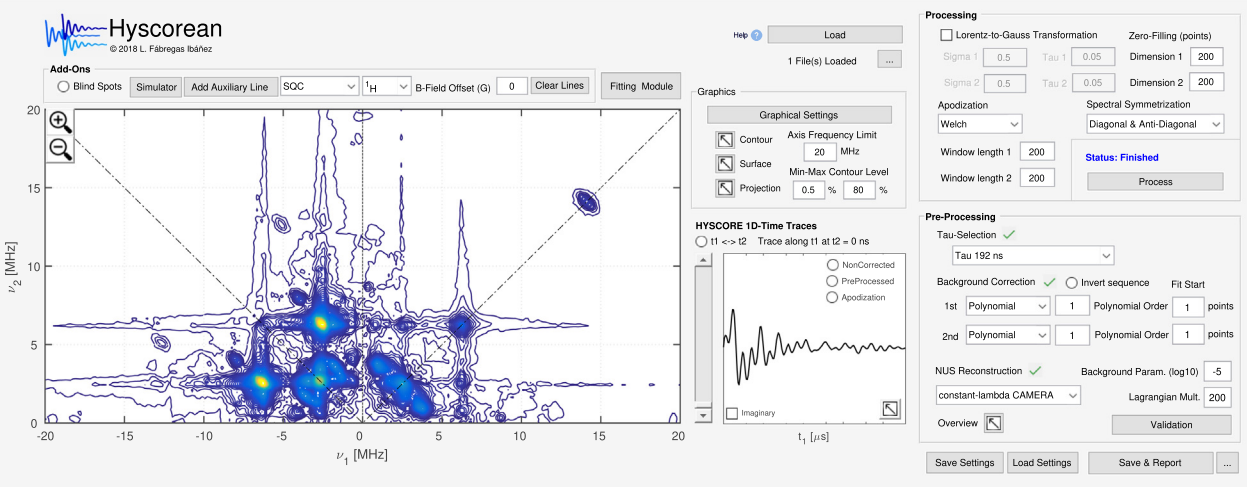

Fig. 3. Screen capture of the main graphical user-interface of Hyscorean. All spectra in this work were processed, analyzed and exported using this interface.

the diagonal, Λ leaves the matrix **X** unchanged, whereas for the symmetrization about the anti-diagonal, Λ flips the columns of **X** in the left-right direction. Since all four quadrants of the HYSCORE spectrum are taken into account, symmetrization about the diagonal, anti-diagonal or about both of them sequentially will yield slightly different results. Best artifact suppression is achieved by symmetrizing about the diagonal and anti-diagonal sequentially. This protocol has to be applied with caution since symmetrization of two crosspeaks with strong Lorentzian ridges (star-effect), extending over a wide range of the spectrum, can introduce false crosspeaks [35]. Lorentz-to-Gauss transformation can attenuate this problem to some extent. Another possibility to enforce symmetry in the reconstructed NUS spectra is the introduction of a symmetry constraint in the reconstruction algorithms. This may, however, lead to suppression of weak peaks which may not be recovered symmetrically. The user may first want to see such peaks before dismissing them in a second step, because other information on the sample could make it likely that they are true positives. Additionally, enforcing symmetrization as a post-processing step is algorithm independent and can be applied to uniformly-sampled spectra as well. All further spectra presented in this work are symmetrized about their diagonal and anti-diagonal.

3.2. Validation of NUS HYSCORE spectra

There exist so far no criteria for the optimal parameter choice for the different reconstruction methods. Hence, this choice becomes another source of uncertainty and error. Spectral reconstruction methods are regularization methods, hence the relation between the input and the resulting error is non-linear and no analytical theory exists to predict uncertainty of the peaks in the spectrum. Validation allows the estimation of this uncertainty by numerical tests. This has already been proven to be a powerful approach to estimate the uncertainty of regularization results obtained for pulsed dipolar spectroscopy (PDS) [36].

Here we propose validation of NUS HYSCORE spectra by numerically testing those parameters, from which uncertainty may arise: background parameter and Lagrange multiplier of maxEnt methods, the threshold parameter of IST methods, background correction, noise and sampling density. The numerical validation tests are performed analogously to the validation offered by the DeerAnalysis [37] software: different parameter sets are defined and the experimental data is processed to give a set of spectra which are then analyzed statistically to yield the estimated uncertainty as well as lower and upper bounds to the spectra. Validation of NUS HYSCORE spectra may reveal false positives caused by sampling artifacts or false negatives caused by background correction or spectral reconstruction. This also offers the possibility to assess the stability of the NUS reconstruction results for a given parameter range.

4. Hyscorean

Hyscorean is a graphical-user interface (GUI) MATLAB-based program, which implements the processing of experimental HYSCORE data of uniform or non-uniform nature. The GUI shown in Fig. 3 allows for a highly interactive and reproducible processing of HYSCORE data. All reconstruction methods and processing tools presented in this work are implemented along standard signal processing techniques such as background correction, zero-filling, apodization and Lorentz-Gauss transformation required for the correct processing of HYSCORE signals. Hyscorean also offers a module for the validation of HYSCORE spectra originating either from uniform or non-uniform sampling.

Once the HYSCORE spectra are processed, they can be analyzed via Hyscorean's fitting module based on EasySpin simulations [38]. The user is only required to define the spin system as Hyscorean automatically constructs the remaining EasySpin structures from experimental and processing parameters of the spectrum to be fitted. The fitting of single spectra or simultaneous fitting of multiple spectra is facilitated by the module's GUI. Importantly, the software employs the same processing parameters for the simulated signals as for the experimental data. This way, the fitting of certain spectral linewidths and features is expected to improve both in precision and performance. Additionally, a new interactive spectral weighting tool is provided which allows the fitting of challenging spectral regions or features. The NUS schedule generator and spectrometer control files are provided as stand-alone files in the package. An extensive manual describes all features of Hyscorean in detail.

5. NUS EPR experiments

EPR experiments can only benefit from NUS if the spectrometer hardware and software are capable of realizing such experiments. NUS experiments are easier to implement on home-built EPR spectrometers controlled by home-written software due to the enormous freedom they provide. Nonetheless, these spectrometers

are available only to a few research groups. The current generation of commercial Bruker EPR spectrometers does not readily allow for NUS experiments implementation. Therefore, we have developed a workaround to perform NUS experiments on commercial Bruker spectrometers controlled by the XEPR software.

To achieve this we have exploited the limited flexibility offered by the pulse spectroscopy language (PulseSPEL) and the procedure description language (ProDeL) available in XEPR. The main idea behind our approach is depicted graphically in Fig. 4.

Algorithm 1. Pseudo-code algorithm for the proposed ProDeL program for NUS HYSCORE measurements on commercial Bruker spectrometers.

input: NUS schedule in BES3T format
output: 1D-dataset with the abcissa encoding the NUS timings and the ordinate containing the complex NUS signal intensities
Load NUS schedule as a dataset and get the t_1 and t_2 timings;
for *all τ-values to be measured* **do**
  Set PulseSPEL delay `d1` to current τ-value;
  while *number of points in dataset less than length of timings schedule* **do**
    Run experiment in PulseSPEL file measuring fourteen points;
    Set fourteen t_1-t_2 timing pairs to the `d4-d31` PulseSPEL delays;
    if *remaining points to be measured are less than fourteen* **then**
      Set overflow points to dummy values.
    end
    Encode these t_1-t_2 timing pairs to the dataset abscissa according to (7) ;
  end
  Save non-dummy measured points to the dataset ordinate;
end

The NUS experiment is controlled by a home-written ProDeL program, which takes a set of HYSCORE points from an externally generated NUS schedule. For each set of points, the program then sets the corresponding timings of a home-written PulseSPEL program, which is then loaded into the pulse forming unit to measure the set of HYSCORE points. Once the set of points is returned from the spectrometer, the ProDeL program writes them into a hidden dataset according to the NUS schedule. Once all points in the schedule have been measured, this dataset is loaded into the XEPR user-interface from where the data can be saved.

A more detailed description of the program is given in Algorithm 1 in pseudo-code form, describing how the program constructs a one-dimensional dataset representing the sparse two-dimensional NUS HYSCORE signal. On each run only fourteen points can be measured as PulseSPEL provides a limited amount of delay variables. The variables d0-d3 are reserved for other required delays, leaving delays d4-d31 for fourteen NUS HYSCORE timings. As described in Algorithm 1, the NUS timing pairs (t_1, t_2) are encoded into the abscissa values X_{Abs} according to

$$X_{\text{Abs}}(t_1, t_2) = t_2 + \frac{t_1}{10,000}. \tag{7}$$

Due to the limited resolution of the PatternJet raster (2 ns or 4 ns depending on the version), any (t_1, t_2) timing combination mapped via (7) will result in the t_1-timings being always encoded in the decimal part of the abscissa values and the t_2-timings as the integer part, assuming here that no HYSCORE t_1-timing exceeds 10 µs. This way Hyscorean recovers the timings from which the NUS grid is reconstructed. In a second step, the two-dimensional NUS signal is decoded from the one-dimensional dataset ordinate. The ProDeL and PulseSPEL programs are available along with the Hyscorean package (a copy of the source code can be found in SI). A guide on how these experiments are set up can be found in the Hyscorean manual. This software can also be easily adapted to perform other one- or two-dimensional NUS EPR experiments, e.g. DEER, ESEEM, TRIER, relaxation measurements, etc.

Repeated execution of PulseSPEL-based measurements from ProDeL causes significant communication overhead that reduces effective time for signal acquisition. Therefore, the ProDeL NUS program has been optimized to reduce the overhead communication and the computation times. The performance of these new ProDeL-based NUS measurements was tested against uniform-sampled XEPR measurements for the same amount of measured points on different Bruker spectrometers: equipped with a trans-

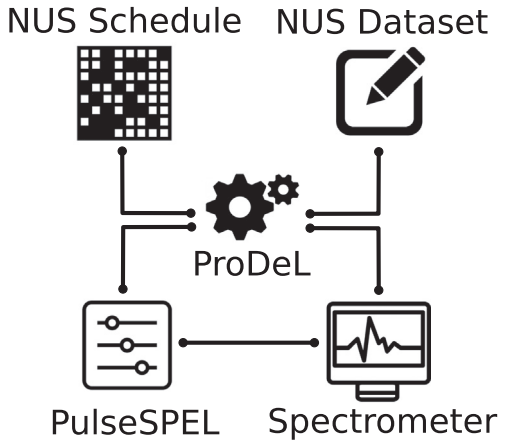

Fig. 4. Schematic of NUS measurements on commercial Bruker spectrometers. The ProDeL program takes the HYSCORE timings from the NUS schedule, updates pointwise the HYSCORE PulseSPEL program and sends it to the spectrometer. The ProDeL program stores the measured points in the NUS dataset and starts the procedure anew until the NUS schedule is completed.

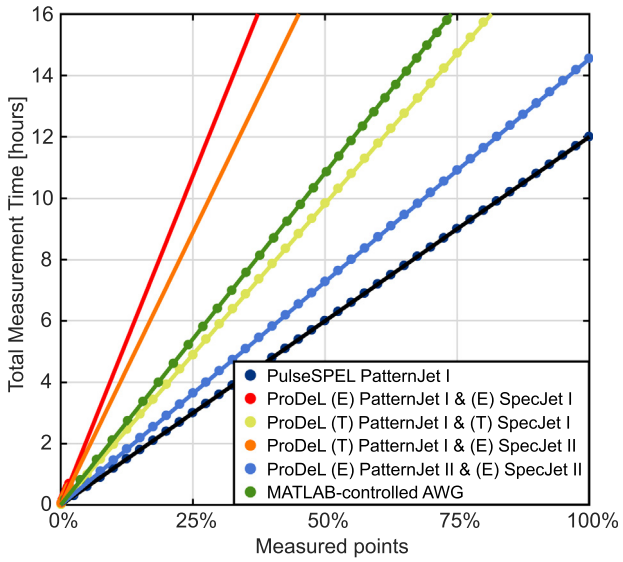

Fig. 5. Measurement time comparison between standard PulseSPEL measurements and the home-written ProDeL program for NUS measurements at different Bruker spectrometers equipped with different combinations of PatternJet and SpecJet connected by transputer (T) or ethernet (E) interfaces. The measurements were performed using 130 scans and 2 µs repetition time. The measurement times are given as colored dots and their corresponding linear fits as colored lines (see legend). The time required for standard PulseSPEL measurements is displayed as a black line. The colored lines represent the experimental measurement times obtained for increasing number of HYSCORE points. As a second reference, the measurement times for our home-built AWG spectrometer [39] are given as a.dark green line. (For interpretation of the references to colour in this figure legend, the reader is referred to the web version of this article.)

puter or ethernet-connected PatternJet I or II and transputer or ethernet-connected SpecJet I or II. The results in Fig. 5 show that the ProDeL-based NUS measurements require more time per point than the uniform measurements obtained only via PulseSPEL. The measurements performed on the transputer PatterJet I and SpecJet I spectrometer are much slower (about 60–65%) than the standard measurements. On two other PatternJet I-based spectrometers with ethernet or mixed communication the performance strongly drops (executing about 300% slower) rendering NUS on such machines almost impractical. In contrast, on the ElexsysII spectrometer equipped with PatternJet II and SpecJet II and full ethernet communication, the ProDeL program executes only about 20% slower per data point than a standard uniform-sampled measurement, which still allows for practical NUS experiments with quite significant measurement time reductions. This difference arises from the distinct speeds of connection between the different components in these spectrometers. In particular, a clear difference arises between the two PatternJet generations. As a consequence of these results, a different sampling density threshold (depending on the machine) exists for which NUS experiments are expected to yield longer measurement times than their uniform counterparts. We additionally tested NUS on our home-built MATLAB-controlled AWG spectrometer [39] with home-written MATLAB scripts, which yielded slower performance for normal measurements due to the pulse sequence compilation times required (see Fig. 5). However, NUS measurements on this spectrometer do not lead to any additional overhead.

6. Case study

As a proof of concept, HYSCORE spectra of low-spin iron(III) species after ethyl diazoacetate (EDA) addition to a myoglobin variant called Mb*(NMH) [40], were measured. The sample is of current research interest and was prepared according to [40] (see also SI Experimental Methods). Both uniformly and non-uniformly sampled HYSCORE spectra were acquired on two different commercial Bruker X-band spectrometers, using the NUS ProDeL program. The spectra were recorded at two different magnetic fields (see Fig. S1 for the echo-detected spectrum), and exhibit a variety of peaks with a large dynamic range. For the sake of comparison, all experimental parameters were kept identical

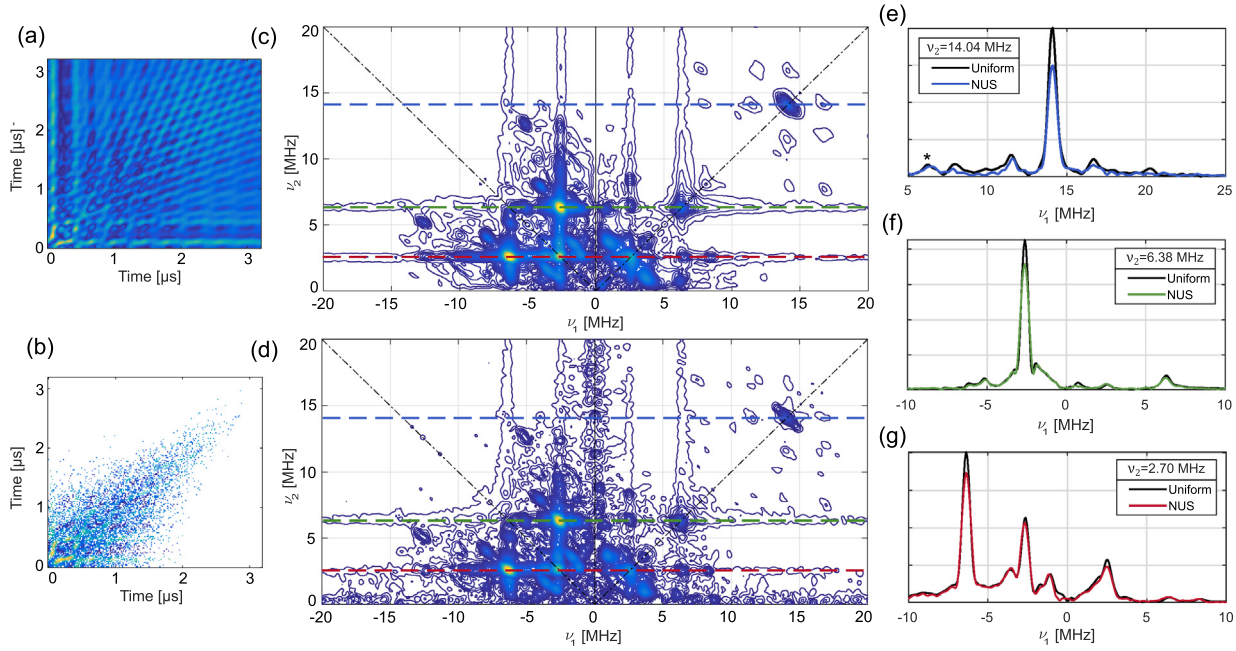

Fig. 6. Experimental HYSCORE magnitude spectra measured uniformly and non-uniformly at 3296 G. The uniform signal (a) was processed into spectrum (c), whereas sampling 15% of the signal (b) yielded spectrum (d) via FFM-CG reconstruction ($\log_{10}(\delta) = -4$). Cross-sections along the first dimension ν_1 indicated by the dashed colored lines in the HYSCORE spectra are shown at (e) $\nu_2 = 14.04$ MHz, (f) $\nu_2 = 6.38$ MHz and (g) $\nu_2 = 2.70$ MHz. The peak in (e) marked by an asterisk corresponds to a 1D-peak arising from the Lorenztian-tail of a diagonal peak. All cross-sections were scaled with respect to the corresponding noise level. All corresponding processing parameters can be found in Table S2 and the experimental parameters in Table S1.

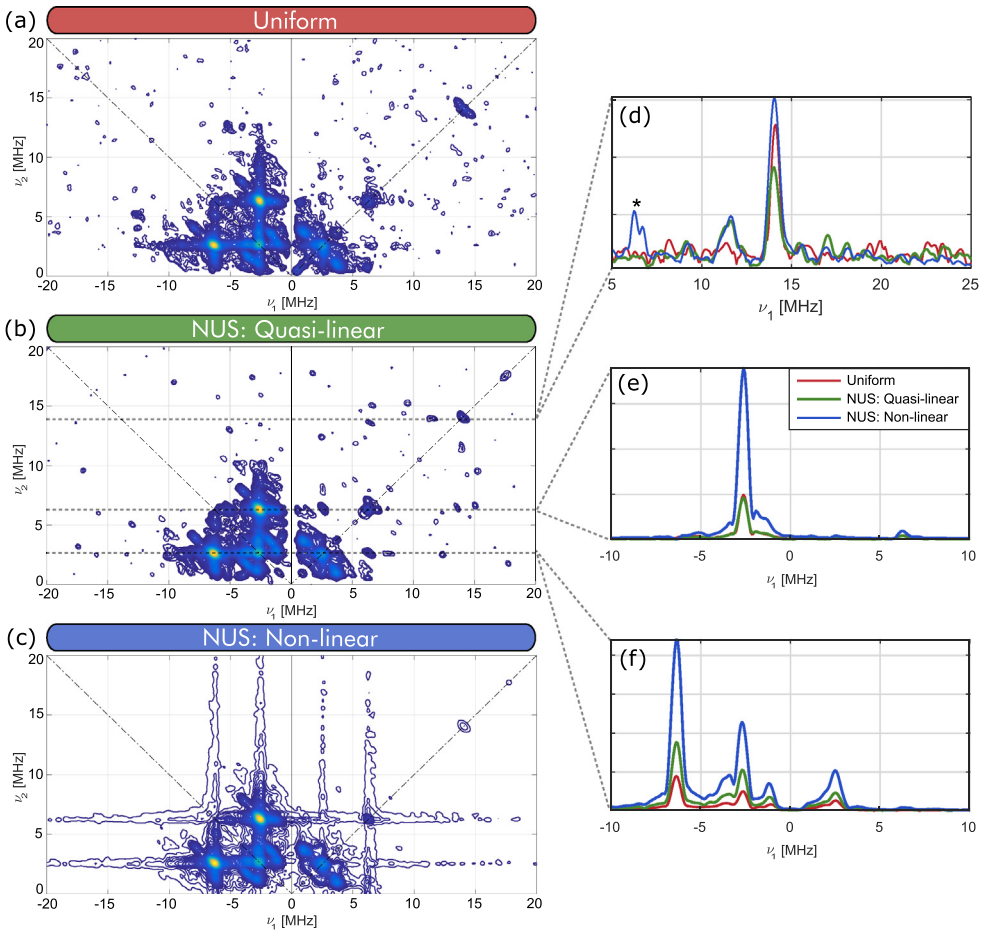

Fig. 7. Experimental HYSCORE magnitude spectra measured uniformly and non-uniformly at 3296 G with added white noise of 25% of the maximal signal intensity. The noisy uniform signal was processed into spectrum (a). The noisy NUS signal was reconstructed (b) linearly via IST-D and (c) non-linearly via constant-λ CAMERA using $\lambda = 80$ and $\log_{10}(\delta) = -4$. Cross-sections along the first dimension ν_1 indicated by the dashed lines in the HYSCORE spectra are shown at (d) $\nu_2 = 14.04$ MHz, (e) $\nu_2 = 6.38$ MHz and (f) $\nu_2 = 2.70$ MHz. The peak in (d) marked by an asterisk corresponds to a 1D-peak arising from the Lorenztian-tail of a diagonal peak. All cross-sections were scaled with respect to the corresponding noise level. For the sake of clarity the minimal contour level for the (a) and (b) was set to 2% of the maximal intensity, whereas for (c) it could be kept at 0.5%.

between the NUS and uniform measurements (see Table S1 for experimental parameters). The NUS measurements were performed using diagonal-exponential EMS [26] with a decay time of half of the grid size. The grid itself was set to 200x200 points with a resolution of 16 ns (see Fig. 6b). The pseudo-random numbers were generated in MATLAB by Latin hypercube sampling (LHS) [41] with a fixed seed to ensure reproducibility.

The NUS spectrum at 3296 G (see Fig. 6d) was recorded on an Elexys spectrometer equipped with an ethernet-connected PatternJet I in 13 h in contrast to the 25 h required for the uniform case. The NUS spectrum at 3456 G (see Fig. S2) was recorded on an Elexys spectrometer equipped with a transputer-connected PatternJet I in approximately 6 h in contrast to the 26 h required for the measurement of the uniform spectrum. The experimental measurement times required for the NUS experiments largely exceed the times which would be expected for the sampling density of 15% employed. As discussed above, this arises from the communication overhead during ProDeL program execution.

6.1. Experimental results

Comparison between uniformly sampled and NUS HYSCORE spectra in Fig. 6 and SI Fig. S2 shows that the reconstruction of the HYSCORE spectra from the 15% NUS signal recovers all crosspeaks and features present in the uniform case. All investigated reconstruction methods seem to yield similar results, as in all cases all crosspeaks were recovered (see Fig. S4). In the NUS reconstruction, however, the peak ridges as well as the shape of some less intense peaks appear to be somewhat distorted. A prominent difference arising in the NUS spectra is the presence of multiple strong artifacts along the zero-frequency axes, which we attribute to imperfect background correction (due to the reduced amount of points available for fitting) coupled to the NUS reconstruction. In order to test this, the NUS spectrum was validated for the background correction parameters. Validation of a large set of background correction trials reveals that these artifacts are indeed caused by the background correction (see Fig. S3) and are therefore not of statistical relevance. Further validation of the sampling density reveals that the spectrum is stable down to 10% sampling density, an indication that our findings are not limited by the used experimental conditions. A conservative choice of sampling density allows this kind of validation, which would not be possible if the spectra would be under sampled (which would result in a high uncertainty in the validation).

6.2. Quasi-linear vs. Non-linear reconstruction

For the NUS HYSCORE spectra in Figs. 6 and S2 no preference can be found for any reconstruction method since all of them exhibit similarly good performance. This is, however, a consequence of the good signal-to-noise ratio of the time-domain data and of the relatively conservative sampling density. Thus, we present a good

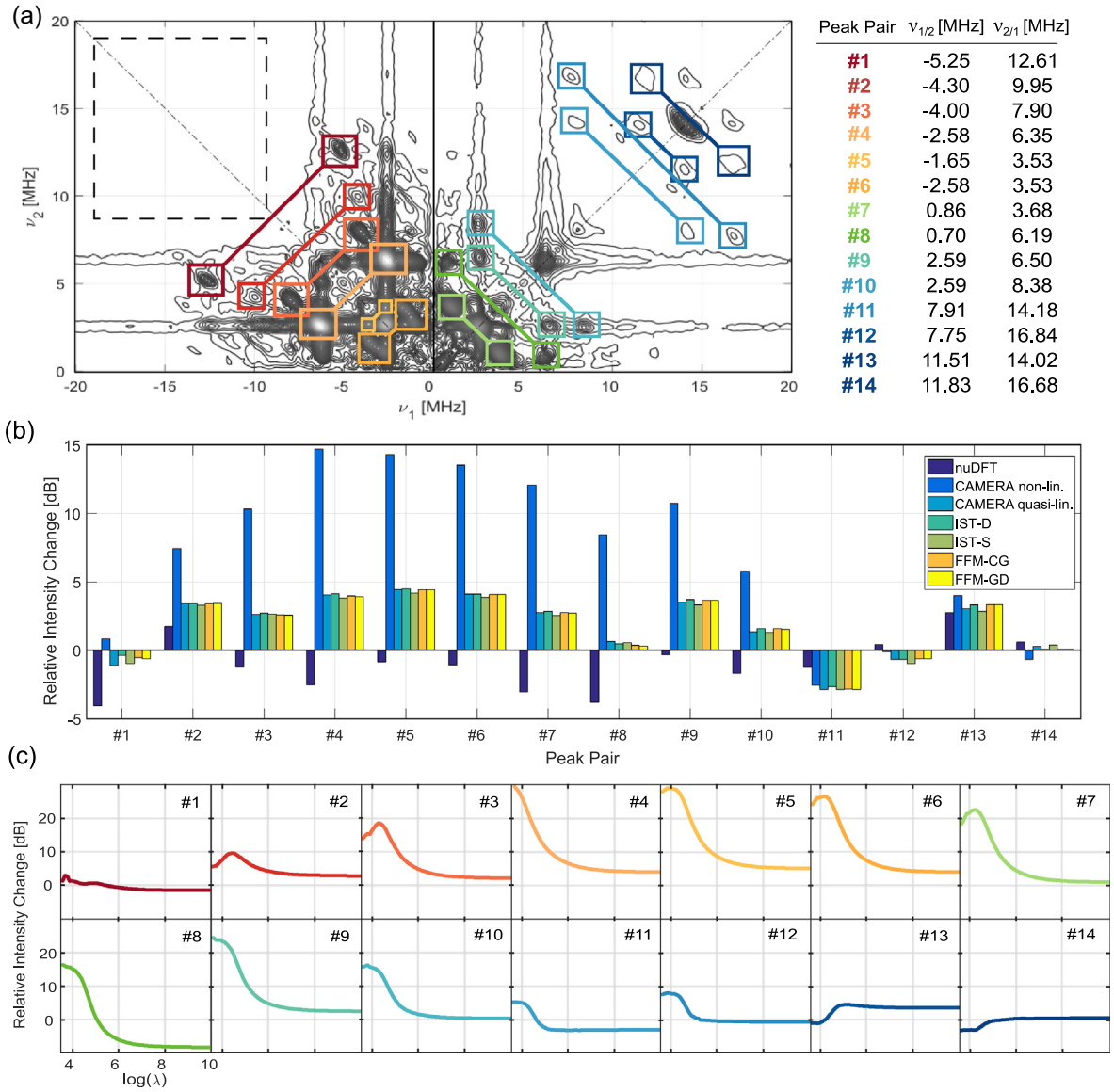

Fig. 8. Analysis of the spectral reconstruction of the NUS signal with added 25% noise level in terms of the relative intensity (peak intensity relative to baseline noise) of the different peaks. In (a) the uniform-sampled spectrum (as in Fig. 6c) is displayed as grey-scale contours. The peak pairs selected for the analysis are highlighted by coloured squares connected by a line and given as a table next to the spectrum. The black dashed box represents the spectral region employed to determine the baseline noise. (b) Performance comparison of the different reconstruction methods (see legend). The bars indicate the relative change in intensity of the peaks on a dB-scale obtained by reconstruction of the noisy NUS signal relative to the noisy uniform case. For the maxEnt methods $\log_{10}(\delta) = -5$ was employed and in CAMERA $\lambda = 5000$ and $\lambda = 150$ were set for the linear and non-linear cases, respectively. (c) Relative change in intensity of the peaks obtained by constant-λ CAMERA reconstruction for different values of the Lagrange multiplier λ at a fixed value of background parameter $\log_{10}(\delta) = -5$ with respect to the uniform case. The lines are colour-coded as their corresponding pe.ak pairs in (a).

example of a stable NUS HYSCORE measurement, where significant reduction in measurement time could be achieved without introducing additional uncertainty into the spectrum. Still, in order to show the performance of the reconstruction methods under more harsh conditions, we artificially added white noise to the experimental data. The noise was scaled to 25% of the maximal signal intensity. In the resulting uniform spectrum in Fig. 7a the noise artifacts now appear at a similar level as many of the crosspeaks, which were previously observable (compared to Fig. 6d). If compared with the same contour levels (see Fig. S4), most weak peaks in the spectrum are completely obscured by noise. With such an example at hand we can now analyze the difference between quasi-linear and strongly non-linear reconstruction.

The noisy NUS signal can be reconstructed using any of the quasi-linear methods (IST-S, IST-D, FFM and constant-λ CAMERA operated at large λ-values) to recover the spectrum in Fig. 7b. As expected from quasi-linear reconstruction, the strict preservation of the experimental data in these methods introduces strong noise and sampling artifacts in the spectrum with intensities similar to some true crosspeaks (see Figs. S5 and S6). However, quasi-linear reconstruction methods still regularize the spectrum, as evident from lower noise and artifact level compared to the uniform case.

Processing with highly non-linear constant-λ CAMERA (i.e. at very low λ-values) yields a different result, since non-linear reconstruction can reduce weighting of the residual term in (3). Using small λ-values, the spectrum is successfully reconstructed by highly non-linear constant-λ CAMERA in Fig. 7c, removing sampling and noise artifacts to a large extent. The method even achieves the reconstruction of some peaks which could not be differentiated from noise artifacts in the uniform spectrum

(see Fig. 7d). Nonetheless, some less intense peaks are missing in the spectrum when compared to the results in Fig. 6, as their intensities are below the noise level. Also, at this noise level, a pair of true crosspeaks (crosspeak pair #1 in Fig. 8a) can be observed in the uniform case, which, in the NUS case, can neither be observed for linear nor for non-linear reconstruction.

In order to further study the behaviour of quasi-linear and non-linear reconstruction we monitored the relative changes in intensity of certain crosspeaks in the noisy NUS spectra in Fig. 7 relative to the uniform case in Fig. 7a. The relative intensities of the uniform and non-uniform spectral peaks were determined by integrating the crosspeak intensities relative to the noise level in an empty region of the spectrum (see Fig. 8a). On a quantitative level, it can be difficult to ascribe meaning to a comparison of methods that differ in their agreement with the empirical data. An alternative approach to quantitatively compare the different reconstruction approaches would involve the computation of receiver operating characteristic (ROC) curves and their associated metrics as proposed by Zambrello et al. for multidimensional NUS NMR [42]. This approach relies on the use of automatic peak selectors as part of the computation of the ROC curves. However, in HYSCORE spectra, due to the presence of ridges (and, if Lorentz-Gauss transformation is omitted, star-effects), selection of peaks is not as straightforward as for multidimensional NMR spectra.

Thereby, as a benchmark test, the relative changes in intensities were monitored for all crosspeaks under reconstruction using all methods discussed in this work. Additionally, we monitored the nuDFT processing as a worst case reference. The results summarized in Fig. 8b show that the nuDFT spectrum results in a considerable loss in relative intensity. All reconstruction methods recover this loss except for peaks, which have fallen below the noise level (peaks 11–14 in Fig. 8b) and for which reconstruction is not successful. Another clear difference between quasi-linear and non-linear reconstruction arises: methods operating in the quasi-linear regime recover all peaks with similar relative intensities. However, the relative gain in intensity is considerably reduced in contrast to strongly non-linear reconstruction (constant-λ CAMERA operated at $\lambda = 150$). Instead a common feature of non-linear reconstruction concerns the expansion of the dynamic range. For non-linearly operated constant-λ CAMERA, the most intense peaks experience a larger change in intensity compared to the less intense ones. Already in spectra with moderate dynamic ranges this becomes a delicate balance and needs to be taken care of.

From all reconstruction methods considered, CAMERA allows a precise control of the reconstruction's non-linearity by adjustment of λ. We monitored the relative intensity changes of the crosspeaks for different values of the Lagrange multiplier λ in the constant-λ mode of CAMERA in Fig. 8c. For all peaks the reconstruction converges to the quasi-linear regime in the limit of large values of λ. For small λ-values the reconstruction becomes highly non-linear, and the relative intensities of the peaks are largely improved (e.g. peaks 3–10 in Fig. 8) with exception of the less intense peaks (e.g. peaks 13–14 in Fig. 8), which become suppressed instead of enhanced. In fact, this tunability is what allows CAMERA to better recover the significant features of the true spectrum from very noisy signals such as this one. However, for very small λ-values, i.e. a strong non-linearity, the visual quality of the spectrum seems to improve drastically. In such a case (see Fig. 9) the star-shaped ridges of the peaks appear to be recovered without any trace of noise left. Such strongly non-linear reconstruction can, however, become a poisonous apple since even strong peaks can begin to be suppressed.

This is best exemplified in Fig. 9, where at $\lambda = 25$ almost all peaks with exception of the strongest ones have been suppressed. In such cases validation comes in handy to identify such false negatives. A quick validation of the Lagrange multiplier, over the values under which the reconstructed spectrum undergoes most changes, yields the results summarized in Fig. 10. From the mean spectrum most false negatives with respect to the reconstruction using $\lambda = 25$ can be identified. The lower and upper bounds give an estimate of the features in the spectrum which undergo most changes for different values of the Lagrange multiplier. Features which appear in the lower bound are the most reliable and certain results. Signals which appear in the mean and the upper bound spectra, have a higher probability to correspond to significant features, whereas signals that appear only in the upper bound spectrum are the most probable to be non-significant. This is most easily interpreted when observing the individual cross-sections,

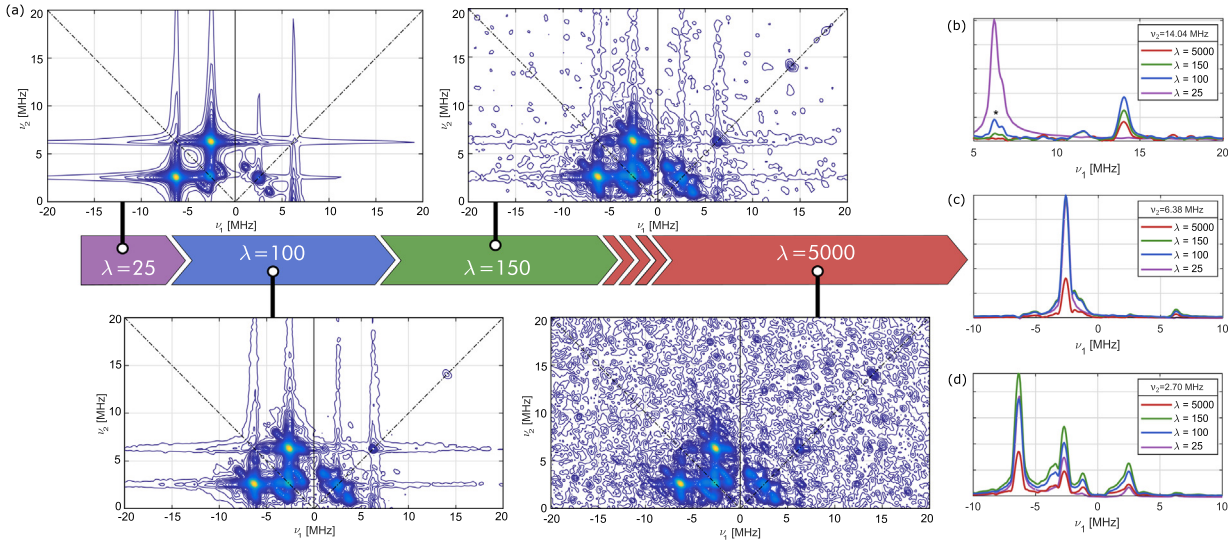

Fig. 9. Effects of non-linearity on NUS reconstruction using constant-λ CAMERA. At small λ-values only the most intense peaks are recovered, decreasing the dynamic range with increasing λ-values until the reconstruction becomes linear. Four NUS HYSCORE spectra are displayed along this evolution for $\lambda = 25, 100, 150, 5000$ ($\log(\lambda) = 3.2, 4.6, 5.0, 8.5$) using a constant background parameter of $\log_{10}(\delta) = -5$. The cross-sections along the first dimension ν_1 of the mean spectrum are shown at (b) $\nu_2 = 14.04$ MHz, (c) $\nu_2 = 6.38$ MHz and (d) $\nu_2 = 2.70$ MHz. The peaks in (b) marked by an asterisk correspond to 1D-peaks arising from the Lorenztian-tail of a diagonal peak.

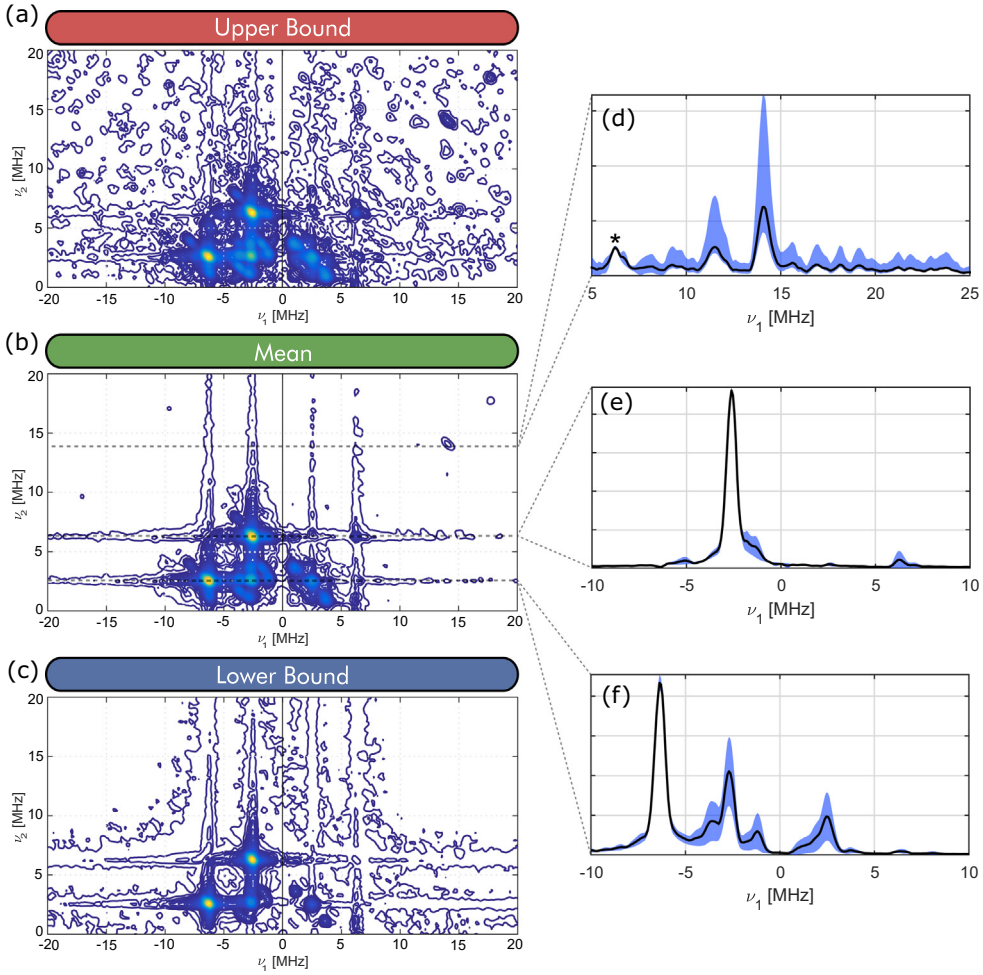

Fig. 10. Results of the validation of the reconstruction of the noisy NUS spectrum using constant-λ CAMERA. The reconstruction was validated for 30 different Lagrange multiplier vales in the range $\lambda = 10$—200. The upper (a) and lower (c) bounds were computed according to the three-sigma rule and their spectra displayed with the same contour levels as the mean spectrum (b). The cross-sections along the first dimension ν_1 of the mean spectrum are shown at (d) $\nu_2 = 14.04$ MHz, (e) $\nu_2 = 6.38$ MHz and (f) $\nu_2 = 2.70$ MHz. The peak in (d) marked by an asterisk corresponds to a 1D-peak arising from the Lorenztian-tail of a diagonal peak. All cross-sections were scaled with respect to the corresponding noise level. The confidence intervals defined by the upper and lower bounds are represented as blue shaded areas.

e.g. in Fig. 10d–f, where the confidence intervals given by the upper and lower bounds can be most easily visualized. In the case of the proton signals in Fig. 10d, the signal at $\nu_1 \approx 12$ MHz is revealed by the validation not to be a false positive, which could be harder to interpret from the contour plots directly.

Another prominent feature in Fig. 9 are the star-shaped ridges that appear at lower values of the Lagrange multiplier, which have also been reported for another system [27]. They are most prominent in the examples at $\lambda = 25$ and $\lambda = 100$. These ridges correspond to the tails of the Lorentzian lineshape, which due to the strong suppression of noise and artifacts become visible and prominent. These ridges can, however, become a nuisance due to their possible overlap, which may mimic cross peaks. The results in Fig. S7 show that these ridges can be eliminated by Lorentz-to-Gauss transformation of the reconstructed time-domain signal.

7. Concluding remarks

In this work we have presented a novel method for the acquisition of NUS HYSCORE spectra on commercial Bruker EPR spectrometers, thereby opening the field of EPR to the NUS techniques. While implementation on commercial spectrometers requires a rather involved workaround, performance is good with the most recent commercial hardware. The required measurement files for these experiments are open-source and easily adaptable to any other type of NUS pulse EPR experiments such as electron Spin Echo Envelope Modulation (ESEEM), double electron-electron (DEER) or triple electron resonance (TRIER) spectroscopy to reduce their corresponding experimental times.

During the analysis of our experimental spectra we have shown that for favourable experimental conditions, such as good SNR, reconstruction of the true spectra from the NUS signal poses no major difficulties given the diverse set of methods presented. We have also shown that, at low signal-to-noise ratio, methods such as constant-λ CAMERA, which permit highly non-linear reconstruction, can outperform other methods operating in the quasi-linear regime. CAMERA is a good example of reconstruction method which permits high tunability of the non-linearity conditions giving the spectroscopist precise control over the reconstruction and a transparent approach to validation. These methods are computationally cheap and, therefore, allow for experimenting with parameters during such a validation. We note again that the analysis presented here (and any analysis based on individual spectra) is anecdotal by nature. A full understanding of the limitations will require time and experience of many users. Thus, further work will include the study of different spectra with varied spectral features and peak linehapes to obtain a more broad understanding of the performance of NUS HYSCORE.

All measurement, processing and analysis tools are provided in the form of a software package "Hyscorean", which can be downloaded from our homepage www.epr.ethz.ch/software.html along with the experimental data analyzed in this work as an example. We hope that this work will encourage the EPR community to apply non-uniform sampling and profit from the sensitivity gain.

Acknowledgments

This work was supported by the ETH Zurich with grant ETH-35 18-2.

Appendix A. Supplementary material

Supplementary data associated with this article can be found, in the online version, at https://doi.org/10.1016/j.jmr.2019.106576.

References

[1] S.V. Doorslaer, Hyperfine spectroscopy: ESEEM, in: eMagRes, American Cancer Society', 2017, pp. 51–70, https://doi.org/10.1002/9780470034590.emrstm1517.
[2] M.W. Maciejewski, H.Z. Qui, I. Rujan, M. Mobli, J.C. Hoch, Nonuniform sampling and spectral aliasing, J. Magn. Reson. 199 (1) (2009) 88–93, https://doi.org/10.1016/j.jmr.2009.04.006.
[3] G.L. Bretthorst, Nonuniform sampling: bandwidth and aliasing, Concepts Magn. Reson. Part A 32A (6) (2008) 417–435, https://doi.org/10.1002/cmr.a.20125.
[4] J.C. Hoch, M.W. Maciejewski, M. Mobli, A.D. Schuyler, A.S. Stern, Nonuniform sampling in multidimensional NMR, in: eMagRes, American Cancer Society, 2012, pp. 181–195, https://doi.org/10.1002/9780470034590.emrstm1239.
[5] M. Mobli, M.W. Maciejewski, A.D. Schuyler, A.S. Stern, J.C. Hoch, Sparse sampling methods in multidimensional NMR, Phys. Chem. Chem. Phys. 14 (31) (2012) 10835–10843, https://doi.org/10.1039/C2CP40174F.
[6] J.C. Hoch, M.W. Maciejewski, M. Mobli, A.D. Schuyler, A.S. Stern, Nonuniform sampling and maximum entropy reconstruction in multidimensional NMR, Acc. Chem. Res. 47 (2) (2014) 708–717, https://doi.org/10.1021/ar400244v.
[7] V.Y. Orekhov, I. Ibraghimov, M. Billeter, Optimizing resolution in multidimensional NMR by three-way decomposition, J. Biomole. NMR 27 (2) (2003) 165–173, https://doi.org/10.1023/A:1024944720653.
[8] V.Y. Orekhov, V.A. Jaravine, Analysis of non-uniformly sampled spectra with multi-dimensional decomposition, Prog. Nucl. Magn. Reson. Spectrosc. 59 (3) (2011) 271–292, https://doi.org/10.1016/j.pnmrs.2011.02.002.
[9] A. Shchukina, P. Kasprzak, R. Dass, M. Nowakowski, K. Kazimierczuk, Pitfalls in compressed sensing reconstruction and how to avoid them, J. Biomol. NMR 68 (2) (2017) 79–98, https://doi.org/10.1007/s10858-016-0068-3.
[10] I. Drori, Fast minimization by iterative thresholding for multidimensional NMR spectroscopy, EURASIP J. Adv. Signal Process. 2007 (1) (2007) 020248, https://doi.org/10.1155/2007/20248.
[11] S.G. Hyberts, A.G. Milbradt, A.B. Wagner, H. Arthanari, G. Wagner, Application of iterative soft thresholding for fast reconstruction of NMR data non-uniformly sampled with multidimensional poisson gap scheduling, J. Biomol. NMR 52 (4) (2012) 315–327, https://doi.org/10.1007/s10858-012-9611-z.
[12] S. Sun, M. Gill, Y. Li, M. Huang, R.A. Byrd, Efficient and generalized processing of multidimensional NUS NMR data: the NESTA algorithm and comparison of regularization terms, J. Biomol. NMR 62 (1) (2015) 105–117, https://doi.org/10.1007/s10858-015-9923-x.
[13] A.S. Stern, D.L. Donoho, J.C. Hoch, NMR data processing using iterative thresholding and minimum l1-norm reconstruction, J. Magn. Reson. 188 (2) (2007) 295–300, https://doi.org/10.1016/j.jmr.2007.07.008.
[14] J. Skilling, R.K. Bryan, Maximum entropy image reconstruction – general algorithm, Monthly Not. Roy. Astron. Soc. 211 (1984) 111, https://doi.org/10.1093/mnras/211.1.111.
[15] J.A. Fessler, B.P. Sutton, Nonuniform fast Fourier transforms using min-max interpolation, IEEE Trans. Signal Process. 51 (2) (2003) 560–574, https://doi.org/10.1109/TSP.2002.807005.
[16] J.-Y. Lee, L. Greengard, The type 3 nonuniform FFT and its applications, J. Comput. Phys. 206 (1) (2005) 1–5, https://doi.org/10.1016/j.jcp.2004.12.004.
[17] A. Dutt, V. Rokhlin, Fast Fourier transforms for nonequispaced data, SIAM J. Sci. Comput. 14 (6) (1993) 1368–1393, https://doi.org/10.1137/0914081.
[18] S.G. Hyberts, G.J. Heffron, N.G. Tarragona, K. Solanky, K.A. Edmonds, H. Luithardt, J. Fejzo, M. Chorev, H. Aktas, K. Colson, K.H. Falchuk, J.A. Halperin, G. Wagner, Ultrahigh-resolution 1H–13C HSQC spectra of metabolite mixtures using nonlinear sampling and forward maximum entropy reconstruction, J. Am. Chem. Soc. 129 (16) (2007) 5108–5116, https://doi.org/10.1021/ja068541x.
[19] B. Worley, Subrandom methods for multidimensional nonuniform sampling, J. Magn. Reson. 269 (2016) 128–137, https://doi.org/10.1016/j.jmr.2016.06.007.
[20] M.R. Palmer, C.L. Suiter, G.E. Henry, J. Rovnyak, J.C. Hoch, T. Polenova, D. Rovnyak, Sensitivity of nonuniform sampling NMR, J. Phys. Chem. B 119 (22) (2015) 6502–6515, https://doi.org/10.1021/jp5126415.
[21] J.C.J. Barna, E.D. Laue, M.R. Mayger, J. Skilling, S.J.P. Worrall, Exponential sampling, an alternative method for sampling in two-dimensional NMR experiments, J. Magn. Reson. (1969) 73 (1) (1987) 69–77, https://doi.org/10.1016/0022-2364(87)90225-3.
[22] A.D. Schuyler, M.W. Maciejewski, H. Arthanari, J.C. Hoch, Knowledge-based nonuniform sampling in multidimensional NMR, J. Biomol. NMR 50 (3) (2011) 247–262, https://doi.org/10.1007/s10858-011-9512-6.
[23] R.R. Ernst, Sensitivity enhancement in magnetic resonance, in: J.S. Waugh (Ed.), Advances in Magnetic and Optical Resonance, vol. 2, Academic Press, 1966, pp. 1–135, https://doi.org/10.1016/B978-1-4832-3115-0.50008-9.
[24] S.G. Hyberts, H. Arthanari, G. Wagner, Applications of non-uniform sampling and processing, Top. Curr. Chem. 316 (2012) 125–148, https://doi.org/10.1007/128_2011_187.
[25] S.G. Hyberts, H. Arthanari, S.A. Robson, G. Wagner, Perspectives in magnetic resonance: NMR in the post-FFT era, J. Magn. Reson. 241 (2014) 60–73, https://doi.org/10.1016/j.jmr.2013.11.014.
[26] K.K. Nakka, Y.A. Tesiram, I.M. Brereton, M. Mobli, J.R. Harmer, Non-uniform sampling in EPR – optimizing data acquisition for HYSCORE spectroscopy, Phys. Chem. Chem. Phys. 16 (31) (2014) 16378–16382, https://doi.org/10.1039/C4CP02172J.
[27] A.E. Motygullina, M. Mobli, J.R. Harmer, Optimizing the transformation of HYSCORE data using the maximum entropy algorithm, J. Magn. Reson. 301 (2019) 30–39, https://doi.org/10.1016/j.jmr.2019.02.002.
[28] B. Worley, Convex accelerated maximum entropy reconstruction, J. Magn. Reson. 265 (2016) 90–98, https://doi.org/10.1016/j.jmr.2016.02.003.
[29] A.S. Stern, J.C. Hoch, A new approach to compressed sensing for NMR, Magn. Reson. Chem. 53 (11) (2015) 908–912, https://doi.org/10.1002/mrc.4287.
[30] J.C. Hoch, A.S. Stern, D.L. Donoho, I.M. Johnstone, Maximum entropy reconstruction of complex (phase-sensitive) spectra, J. Magn. Reson. 86 (2) (1990) 236–246, https://doi.org/10.1016/0022-2364(90)90256-9.
[31] G.J. Daniell, P.J. Hore, Maximum entropy and NMR—a new approach, J. Magn. Reson. 84 (3) (1989) 515–536, https://doi.org/10.1016/0022-2364(89)90117-0.
[32] N.M. Balsgart, T. Vosegaard, Fast forward maximum entropy reconstruction of sparsely sampled data, J. Magn. Reson. 223 (2012) 164–169, https://doi.org/10.1016/j.jmr.2012.07.002.
[33] Y. Nesterov, Smooth minimization of non-smooth functions, Math. Program. 103 (1) (2005) 127–152, https://doi.org/10.1007/s10107-004-0552-5.
[34] Y. Nesterov, Gradient methods for minimizing composite functions, Math. Program. 140 (1) (2013) 125–161, https://doi.org/10.1007/s10107-012-0629-5.
[35] R. Brüschweiler, F. Zhang, Covariance nuclear magnetic resonance spectroscopy, J. Chem. Phys. 120 (11) (2004) 5253–5260, https://doi.org/10.1063/1.1647054.
[36] G. Jeschke, Dipolar spectroscopy – double-resonance methods, in: eMagRes, American Cancer Society, 2016, pp. 1459–1476, https://doi.org/10.1002/9780470034590.emrstm1518.
[37] G. Jeschke, V. Chechik, P. Ionita, A. Godt, H. Zimmermann, J. Banham, C.R. Timmel, D. Hilger, H. Jung, DeerAnalysis2006—a comprehensive software package for analyzing pulsed ELDOR data, Appl. Magn. Reson. 30 (3–4) (2006) 473–498, https://doi.org/10.1007/BF03166213.
[38] S. Stoll, A. Schweiger, EasySpin, a comprehensive software package for spectral simulation and analysis in EPR, J. Magn. Reson. 178 (1) (2006) 42–55, https://doi.org/10.1016/j.jmr.2005.08.013.
[39] A. Doll, G. Jeschke, Wideband frequency-swept excitation in pulsed EPR spectroscopy, J. Magn. Reson. 280 (2017) 46–62, https://doi.org/10.1016/j.jmr.2017.01.004.
[40] T. Hayashi, M. Tinzl, T. Mori, U. Krengel, J. Proppe, J. Soetbeer, D. Klose, G. Jeschke, M. Reiher, D. Hilvert, Capture and characterization of a reactive haem-carbenoid complex in an artificial metalloenzyme, Nat. Catal. 1 (8) (2018) 578, https://doi.org/10.1038/s41929-018-0105-6.
[41] M. Stein, Large sample properties of simulations using latin hypercube sampling, Technometrics 29 (2) (1987) 143–151, https://doi.org/10.1080/00401706.1987.10488205.
[42] M.A. Zambrello, M.W. Maciejewski, A.D. Schuyler, G. Weatherby, J.C. Hoch, Robust and transferable quantification of nmr spectral quality using iroc analysis, J. Magn. Reson. 285 (2017) 37–46, https://doi.org/10.1016/j.jmr.2017.10.005.